NKCCs in the fibrocytes of the spiral ligament are silent on the unidirectional K+ transport that controls the electrochemical properties in the mammalian cochlea

吉田, 崇正

NKCCs in the fibrocytes of the spiral ligament are silent on the unidirectional K$^+$ transport that controls the electrochemical properties in the mammalian cochlea

Takamasa Yoshida[1,2,3]**, Fumiaki Nin**[1,2]**, Genki Ogata**[1,2]**, Satoru Uetsuka**[1,2,4]**, Tadashi Kitahara**[4,5]**, Hidenori Inohara**[4]**, Kohei Akazawa**[6]**, Shizuo Komune**[3]**, Yoshihisa Kurachi**[7]**, Hiroshi Hibino**[1,2]

[1]Department of Molecular Physiology, Niigata University School of Medicine

[2]Center for Transdisciplinary Research, Niigata University

[3]Department of Otorhinolaryngology, Graduate School of Medical Sciences, Kyushu University

[4]Department of Otorhinolaryngology - Head and Neck Surgery, Graduate School of Medicine, Osaka University

[5]Department of Otorhinolaryngology - Head and Neck Surgery, Nara Medical University

[6]Department of Medical Informatics, Niigata University Medical and Dental Hospital

[7]Division of Molecular and Cellular Pharmacology, Department of Pharmacology, Graduate School of Medicine, and The Center for Advanced Medical Engineering and Informatics, Osaka University

Corresponding author:

H Hibino - Department of Molecular Physiology, Niigata University School of Medicine.

       1-757 Asahimachi-dori, Chuo-ku, Niigata, Niigata 951-8510, Japan.

Email: hibinoh@med.niigata-u.ac.jp, Tel: +81-25-227-2071, Fax: +81-25-227-0460.

Abstract

Unidirectional K^+ transport across the lateral cochlear wall contributes to the endocochlear potential (EP) of +80 mV in the endolymph, a property essential for hearing. The wall comprises two epithelial layers, the syncytium and the marginal cells. The basolateral surface of the former and the apical membranes of the latter face the perilymph and the endolymph, respectively. Intrastrial space (IS), an extracellular compartment between the two layers, exhibits low $[K^+]$ and a potential similar to the EP. This IS potential (ISP) dominates the EP and represents a K^+ diffusion potential elicited by a large K^+ gradient across the syncytial apical surface. The K^+ gradient depends on the unidirectional K^+ transport driven by Na^+,K^+-ATPases on the basolateral surface of each layer and the concomitant $Na^+,K^+,2Cl^-$-cotransporters (NKCCs) in the marginal-cell layer. The NKCCs coexpressed with the Na^+,K^+-ATPases in the syncytial layer also seem to participate in the K^+ transport. To test this hypothesis, we examined the electrochemical properties of the lateral wall with electrodes measuring $[K^+]$ and potential. Blocking NKCCs by perilymphatic perfusion of bumetanide suppressed the ISP. Unexpectedly and unlike the inhibition of the syncytial Na^+,K^+-ATPases, the perfusion barely altered the electrochemical properties of the syncytium but markedly augmented $[K^+]$ of the IS. Consequently, the K^+ gradient decreased and the ISP declined. These observations resembled those when the marginal-cells' Na^+,K^+-ATPases or NKCCs were blocked with vascularly applied inhibitors. It is plausible that NKCCs in the marginal cells are affected by the perilymphatically perfused bumetanide and these transporters but not those in the syncytium mediate the unidirectional K^+ transport.

Introduction

The endolymph in the mammalian cochlea shows 150 mM [K^+] and an endocochlear potential (EP) of +80 mV relative to the perilymph [3, 10] (**Fig. 1A**). Hair cells' basolateral membrane bathe in perilymph while their apical surface and stereocilia are exposed to endolymph. The EP maximizes the sound-induced K^+ entry in hair cells from the endolymph, thereby causing the excitation of the cells [14]. K^+ exits hair cells to the perilymph and is transported unidirectionally back to the endolymph through the lateral cochlear wall comprising the spiral ligament and the stria vascularis (**Fig. 1A**) [47, 52].

The lateral wall is considered as a double-layered epithelial system (**Fig. 1B**). One is a monolayer of strial marginal cells whose apical surfaces face the endolymph. The other is a syncytium comprising fibrocytes in the ligament and intermediate and basal cells in the stria; these three cell types are interconnected by gap junctions and thereby bear similar electrochemical properties [19, 43, 45, 48]. Between the two layers lies a 15 nm extracellular compartment, the intrastrial space (IS), which is transversed by numerous capillaries (**Fig. 1B**) [13, 41]. The IS exhibits a low [K^+] and a potential similar to the EP [15, 35]. This IS potential (ISP) dominates the EP in normal conditions [11, 27, 35].

The EP primarily represents the sum of two K^+ diffusion potentials in the lateral wall [27, 28]. We showed that one diffusion potential governs the ISP and stems from K^+ channels Kir4.1 on the apical surface of the syncytium as expected by other works [2, 45]. The K^+ gradient across the apical surface establishes a large diffusion potential and is maintained by the low [K^+] of the IS and the high [K^+] inside the syncytium ([K^+]$_{Syn}$). The other diffusion potential emerges from I_{Ks} K^+ channels on the marginal-cells' apical membranes.

The unidirectional K^+ transport from the perilymph to the endolymph contributes to the ISP and the EP by controlling [K^+] in various compartments of the lateral wall [28]. This K^+ transport is proposed to be driven primarily by both the NKCCs and Na^+,K^+-ATPases that occur together on the basolateral surfaces of each of the syncytial and the marginal-cell layers [10, 25, 49, 52]. Indeed, inhibiting the syncytial Na^+,K^+-ATPases decreases [K^+]$_{Syn}$, reducing the K^+ gradient across the apical surface and thus the ISP [1]. Critical roles of the marginal-cells' Na^+,K^+-ATPases and NKCCs have been also demonstrated [27]. Contrary to the common assumption, we provide evidence here that the syncytial NKCCs under physiological conditions may barely uptake K^+ and therefore be "silent" on the unidirectional K^+ transport.

Materials and Methods

General information

The experimental protocol was approved by the Animal Research Committees of Niigata University School of Medicine. The experiments were carried out under the supervision of the Committees and in accordance with the Guidelines for Animal Experiments of Niigata University and the Japanese Animal Protection and Management Law.

The electrophysiological assays with living animals were performed with a procedure similar to those in Nin et al [27] and Adachi et al [1] as described below.

Double-barreled K$^+$-selective microelectrode

Electrodes were fabricated from double-barreled borosilicate capillary glass (WPI; Sarasota, FL, USA). A K$^+$ exchanger (IE190; WPI) was inserted into the salinized interior of one barrel. The K$^+$-selective barrel was silanized by vaporized dimethyldichlorosilane (LS-130; ShinEtsu, Tokyo, Japan), filled at the tip with K$^+$-selective liquid ion exchanger (IE190; WPI) and backfilled with 150 mM KCl. The voltage barrel was filled with 150 mM NaCl. Each barrel was connected via an Ag/AgCl electrode to a dual electrometer with high input-resistance (FD223a; WPI).

Calibration of each K$^+$-selective electrode was performed using the following steps. First, the electrode sensitivity was checked at 37 °C with a series of aqueous solutions containing (in mM) 15 KCl, 50 KCl and 150 KCl; the deviation of the slope from the theoretical value was confirmed to be less than 10%. Second, the electrode property was obtained from a series of mixed KCl-NaCl solutions containing (KCl/NaCl, in mM): 1.5/148.5, 5/145, 15/135, 50/100, and 150/0. Then, assuming that the activity coefficients for K$^+$ of these mixed solutions were constant at 0.727 [21], the potentials were plotted as a function of ionic activity of K$^+$ (aK$^+$). The data were fitted with a quadratic function that was then used to convert measured diffusion potentials to aK$^+$ in the experiments. In every assay, standard solution (in mM: 5 KCl, 145 NaCl) was applied to the tympanic cavity and its concentration was measured with K$^+$-selective electrode for its calibration. After the experiment, the electrode was again evaluated with the mixed solutions mentioned above.

Of note, an ionic activity is an effective concentration of an ion, or in other words a measure of the fraction of the ions that are free and active and actually elicit a variety of chemical and biological phenomena including the diffusion potential monitored with the ion-selective electrode. An ionic activity is the product of the ion's concentration and its activity coefficient. Because the coefficient is variable and unmeasurable in intact cells and tissues, the value of the aK$^+$ was measured and reported in this study.

Animals

Male Hartley guinea pigs with normal Preyer's reflex (200-400 g; SLC Inc., Hamamatsu, Japan) were first deeply anesthetized with intraperitoneal injection of pentobarbital sodium (64.8 mg/kg; Somnopentyl; Kyoritsu Seiyaku, Tokyo, Japan). To assess the depth of anesthesia, toe pinch, corneal reflex and respiratory rate were used as a guide. When anesthesia was not sufficient, pentobarbital sodium (5 mg/kg) was further given to the animals. Next, neuromuscular blockage was achieved with intramuscular injection of vecuronium bromide (4 mg/kg), and the animals were artificially ventilated with room air during experiments. Throughout the experiments, body temperature of the animals was maintained at 37 °C by a heating blanket (BWT-100A, Bio Research Center, Nagoya, Japan). The depth of anesthesia was monitored by fluctuations in the heart rate and anesthesia was maintained by additional injection of pentobarbital sodium (10 mg/kg) every 1-1.5 hrs. The animals were sacrificed with an overdose of pentobarbital sodium (400 mg/kg) at the end of the experiments.

In vivo measurement

The cochlea was exposed by a ventrolateral approach and a fenestra (~200 µm in diameter) was made on the bony wall of the second cochlear turn. With an Ag/AgCl wire on the neck muscles as a reference, a K^+-selective microelectrode was inserted into the fenestra and advanced from the perilymph towards the endolymph by a micromanipulator (MP-285; Sutter Instrument Co., Novato, CA, USA) to record both the potential and aK^+ of the lateral cochlear wall. The EP was simultaneously measured by a single-barreled electrode filled with 150 mM KCl; the electrode was inserted through the above fenestra and held in the scala media.

Perilymphatic and vascular application of the blockers

The control solution had the following composition (in mM): 122 NaCl, 24 $NaHCO_3$, 0.5 NaH_2PO_4, 5 KCl, 1.2 $CaCl_2$, 1 $MgCl_2$, 4 glucose, 5 HEPES; bubbled with 5% O_2, 5% CO_2 and 90% N_2 for 30 min; pH 7.4. This solution was used to apply the blockers to the perilymphatic space as well as to the vasculature (see below).

As for perilymphatic perfusion of solutions in the absence or presence of the blockers, inlet and outlet holes were made on the basal cochlear turn of the scala tympani and the third turn of the scala vestibuli, respectively. A silica capillary tube (P/N 062472; SGE Analytical Science, Melbourne, Australia) connected to a syringe was inserted into the inlet hole and sealed with cyanoacrylate glue. The perfusion was performed at a rate of 10 µl/min using a syringe pump (Pump 33; Harvard Apparatus, Holliston, MA, USA). In a preliminary experiment, we found that the EP was relatively unstable for ~10 min after starting the perfusion, probably due to the artifact of initial pressure of the solution's flow (see **Fig. 3Ad**). Therefore, in assays of **Figs. 2**, **3B** and **3C**, we first perilymphatically applied the control solution for approximately 30

min without recording and then advanced the K$^+$-selective electrode across the lateral wall. The control solution was switched to the perfusate containing a blocker by a flow selector (Univentor 8401405; Univentor Ltd., Zejtan, Malta).

Bumetanide (Sigma, St Louis, MO, USA) was dissolved in 1 M NaOH at the concentration of 100 mM [38]. This stock solution was diluted in the control solution before bubbling. The final concentration of bumetanide applied to the perilymph was 100 µM. When 1 M NaOH without the blocker was added to the control solution at the same ratio, the pH after bubbling was ~7.5; the perilymphatic perfusion of this solution negligibly affected the EP. Ouabain (sigma), an inhibitor of Na$^+$,K$^+$-ATPase, was dissolved in distilled water to make the stock solution (100 mM). This solution was diluted with the control solution to 50 µM before the experiments. Note that the two blockers at the concentrations mentioned above barely affected the measurements of aK$^+$ with the K$^+$ exchanger.

For intravenous injection, a 3 ml solution containing 30 mg/kg bumetanide was made from its stock solution and the control solution and applied to the right jugular vein in 3 min [24] through a catheter.

Statistical analysis

Mean ± standard deviation (S.D.) was used as a descriptive statistic. The distributions of the measured values among groups were compared using one-way analysis of variance (ANOVA) followed by Tukey-Kramer post hoc test. A p value of <0.05 was considered significant. All statistical analyses were carried out using JMP 9.0.2 (SAS institute Japan inc., Tokyo, Japan).

Results

Generally, NKCCs carry one K^+, one Na^+, and two Cl^- from extracellular fluid to intracellular space. The perilymphatic perfusion of furosemide or bumetanide, blockers of NKCCs, markedly reduce the EP [12, 23], indicating that the functional transporters are expressed in the lateral wall. Histochemical studies including immunogold microscopic examination revealed that type-1 NKCCs occur on the plasma membrane of fibrocytes in the spiral ligament [5, 26, 49]. The fibrocytes' membrane provide the basolateral surface of the syncytium, which is directly exposed to the perilymph [19, 40] (**Fig. 1B**). These observations suggest that the NKCCs, like the concomitant Na^+,K^+-ATPases, would uptake K^+ from the perilymph to the inside of the syncytium and be crucially involved in the unidirectional K^+ transport through the lateral cochlea wall [10, 25, 52]. The idea could be supported by abnormalities detected in type-1 NKCC knockout mice such as the collapse of the endolymphatic space and hearing loss [9, 29]. However, because these mice lack NKCCs not only in the syncytium but also in the marginal cells, it is impossible to understand separately the roles of the transporters in the former region. In this study, we thereby performed *in vivo* experiments as follows. The ISP is a major contributor to the EP and depends on the IS's $[K^+]$ that is controlled by the K^+ transport [11, 27, 28, 35]. To examine the role of the syncytial NKCCs in the lateral wall, we measured the electrochemical properties of the IS of guinea pigs with double-barreled electrodes that monitor both aK^+ and potential (**Fig. 2**) (as for the reason of measuring aK^+, see **Materials and Methods**). In each experiment, the EP is simultaneously recorded with a single-barreled electrode inserted into the endolymph.

In **Fig. 2A**, the control solution containing no blocker was first perfused to the perilymph of the scala tympani for approximately 30 min (see **Materials and Methods**). Thereafter, the perfusate continued to be applied and the double-barreled electrode was driven from the perilymphatic space towards the endolymph. At the outset of the experiment, we detected that aK^+ and potential fluctuated widely; peak values ranged from 51.9 to 64.2 mM and from +4.0 to +9.5 mV, respectively. This finding is consistent with the syncytial profile that we described previously [1]. On further insertion of the electrode, we recorded a low aK^+ of 5.2 mM that is similar to the value in the perilymph and a highly positive potential of +73.1 mV [1, 15, 27, 35]. These electrochemical properties resemble those in the IS [15, 27, 35]. Anoxia has been known to increase aK^+ in the IS (aK^+_{IS}) and decrease ISP [1, 27]. Therefore, to confirm the position of the electrode, we imposed anoxia on the animal. We obtained the results similar to those observed in other works (**Fig. 2**) [1, 27], assuring that the electrode had entered the IS. As expected, the EP also remarkably decreased [20]. Upon reoxygenation, the EP, ISP and aK^+_{IS} recovered and returned to their initial level. We next perfused the solution containing bumetanide (100 μM) to the perilymph. The ISP began to decrease as soon as the blocker was applied and several minutes later the aK^+_{IS} commenced increasing. These two values gradually changed and became stable around 40 mM and +20 mV in ~30 min. The average aK^+_{IS} and ISP at the steady state were 41.1 ± 3.8 mM and +21.0 ± 3.1 mV, respectively (mean ± S.D.; 11

cochleae). Notably, in the example of **Fig. 2A**, the EP declined more dramatically than the ISP and reached a minimum of -28.9 mV. This potential difference was confirmed when the double-barreled electrode was advanced to the endolymph and recorded essentially the same potential as another electrode placed in the endolymph. These results (**Fig. 2A**) resemble the alteration of the IS's properties and EP when the NKCCs on the basolateral surface of the marginal cells were directly inhibited by vascular injection of bumetanide (30 mg/kg; **Fig. 2B**) and those when the Na^+,K^+-ATPases on the same membrane domain were blocked by vascular perfusion of ouabain or by anoxia [27] (for effect of anoxia, see Kuijpers and Bonting [22]). However, the delayed increase of aK^+_{IS} relative to the ISP reduction occurred exclusively in the case of the perilymphatic perfusion of bumetanide. Also, this perturbation altered the properties of the IS and the EP more slowly than the vascular injection (**Figs. 2A** and **2B**) [46]. Of note, the vascularly applied reagents might mainly reach the marginal-cells' basolateral surface and the syncytial apical surface but only modestly the syncytial basolateral surface, because the capillaries in the stria vascularis form the densest network in the lateral wall [39] (**Fig. 1B**). In contrast, blocking the syncytial Na^+,K^+-ATPases that occur together with the NKCCs on the basolateral surface caused different phenotypes (**Fig. 2C**). During perilymphatic perfusion of ouabain (50 µM), the ISP and EP declined in a similar manner whereas the aK^+_{IS} remained nearly constant, as we found previously [1]. The inconsistence between these observations (**Fig. 2C**) and those during the perilymphatic perfusion of bumetanide (**Fig. 2A**) is surprising because on the basolateral surface of the syncytial layer the NKCCs and the Na^+,K^+-ATPases have been assumed to cooperatively uptake K^+ [10, 25, 52] and play similar roles in the K^+ transport.

In our earlier studies, we analyzed the electrochemical properties of the IS during inhibition of the marginal-cells' Na^+,K^+-ATPases with anoxia and demonstrated that the ISP is primarily a K^+ diffusion potential yielded by the K^+ gradient across the apical surface of the syncytium [1, 27], as had previously been suggested [35, 45]. The ISP is described by the following equation

$$\text{ISP} \approx V_{\text{Syn}} + \frac{RT}{F} \cdot \ln\left(\frac{aK^+_{\text{Syn}}}{aK^+_{\text{IS}}}\right),$$

Eq. 1

in which V_{Syn} and aK^+_{Syn} are the potential and intracellular K^+ activity of the syncytium, aK^+_{IS} is the extracellular K^+ activity of the IS, and R, T, and F are the ideal gas constant, absolute temperature, and Faraday constant. Inhibition of the syncytial Na^+,K^+-ATPases, which barely affects aK^+_{IS} (**Fig. 2C**), impairs the ISP by dramatically reducing aK^+_{Syn} [1]. Hence, we concluded that the pumps drive the unidirectional K^+ transport on the basolateral surface of the syncytium. Consequently, to determine the involvement of the NKCCs coexpressed with the Na^+,K^+-ATPases in the K^+ transport, we focused on the electrochemical properties of the syncytium (**Fig. 3**). Generally, it is difficult to maintain a prolonged intracellular recording with an electrode [4, 50]. Nevertheless, it took approximately 30 min to observe the maximum response of the perilymphatic perfusion of the bumetanide to the ISP (**Fig. 2A**). In order to circumvent that problem, we

utilized an approach similar to that of Adachi et al [1] as follows (**Fig. 3**). While the perfusate in the presence or absence of the blockers continued to be applied to the perilymph, the double-barreled K^+-selective electrode was being driven from the perilymph towards the endolymph (1-3 µm/s). With this procedure we cannot continuously monitor the syncytium during the perfusion of the blockers and therefore repetitively inserted the electrodes to the same cochlea multiple times. The EP was simultaneously recorded with the single-barreled electrode placed in the endolymph of the scala media.

As for a control experiment, we tested whether the multiple insertions of the electrodes would affect the electrochemical profile of the lateral wall (**Fig. 3A**). We first measured the profile in physiological conditions (**Fig. 3Aa**). Before entering the IS, the electrode clearly encountered several compartments within the syncytial region that exhibited elevated $a$$K^+$ and potential and thus differed from the perilymph. Some of them showed "flat-topped" peaks with high $a$$K^+$ of 70-80 mM and slightly positive potential of ~+10 mV (*open* and *filled circles*), the hallmark for steady insertion of the electrode into the cells constituting the syncytium [1]. Other compartments showed lower and variable $a$$K^+$ and potential with spike-like appearance. This could have occurred if the electrode penetrated the invaginated processes of the fibrocytes, injured the cells, or was transiently advanced into the cells' small volume of cytoplasm [1]. When the electrode was further advanced, the potential abruptly became highly positive of +65.0 mV and the $a$$K^+$ dropped to the low value similar to the perilymph. It indicates that the electrode had entered the IS [1, 15, 27, 35]. We previously found that, in each experiment, the compartment neighboring the IS consistently exhibited the highest $a$$K^+$ or the nearly highest $a$$K^+$ with the "flat-topped" appearance in the syncytial region and therefore concluded that it likely represents the inside of the syncytium [1]. These measurements were used to quantitatively characterize the electrochemical properties of the syncytium [1] (see **Fig. 3D**). Consistently, within the syncytial region shown in **Fig. 3Aa**, the compartment adjacent to the IS showed the highest $a$$K^+$ of 75.8 mM (*filled circle*). After the IS, further along the electrode insertion, we found that $a$$K^+$ transiently increased to 84.7 mM but then gradually decreased by 30 mM whereas the potential exhibited a similar pattern between the ISP and EP. The peak $a$$K^+$ was lower than the recorded endolymphatic $a$$K^+$ (110.3 mM). Between the IS and the endolymph, there is the marginal-cell layer in which $a$$K^+$ never exceeds the endolymphatic $a$$K^+$ and where the potential is close to the ISP and EP [27]. Therefore, the aforementioned variations in measurement of $a$$K^+$ and potential demonstrate that the electrode penetrates the marginal-cell layer before entering the endolymph.

After retracting the electrode to the perilymph, we perfused the control solution to the perilymph (**Fig. 3Ad**). Then during the perfusion we performed the same assay twice more with different double-barreled electrodes (**Figs. 3Ab** and **Ac**). Notably, in this series of the experiment, the EP remained almost constant (**Fig. 3Ad**). It indicates that physiological conditions of the lateral wall were affected neither by repeated insertions of the electrodes nor by the perfusion of the control solution. However, in the second and third measurements (**Figs. 3Ab** and **3Ac**), the $a$$K^+$ and potential of the

compartment that likely represented the IS were gradually changed and did not stabilize to the typical values observed in our earlier studies [1, 27] (also see **Fig. 2**). This should be owed to the continuous insertion of the double-barreled electrodes. Additionally, the region of the marginal cells was likely undetectable in the second insertion (**Fig. 3Ab**), as we sometimes experienced in our previous work [27]. Nevertheless, in every insertion the properties of the syncytium seemed to be stably recorded because "flat-topped" peaks of $a\mathrm{K}^+$ and potential were clearly detected multiple times within the region prior to the IS (*open* and *filled circles* in **Figs. 3Ab** and **3Ac**). The values of the syncytial compartment adjacent to the IS in the second measurement (70.8 mM and +11.4 mV; **Fig. 3Ab**) and in the third measurement (81.3 mM and +10.6 mV; **Fig. 3Ac**) were similar to those in the first measurement (75.8 mM and +10.4 mV) (*filled circles*; see also **Fig. 3Aa**). We conclude from this control experiment that the procedure is adequate to analyze the properties of the syncytium, although in some occasions it may be unable to precisely measure those of the IS or the marginal cells.

Fig. 3B displays the effect of the perilymphatically perfused bumetanide. In this experiment, we first measured the electrochemical properties of the syncytium with the double-barreled electrode once while applying the control solution (**Fig. 3Ba**). Thereafter, we switched the perfusate to the solution containing bumetanide (100 µM) and inserted different electrodes twice when the EP was reduced to ~+35 mV (**Fig. 3Bb**) and it became stable at ~-53 mV (**Fig. 3Bc**) (see also **Fig. 3Bd**). Overall, the syncytial profiles were likely similar among three measurements. The values of the $a\mathrm{K}^+$ and potential of the syncytial compartment neighboring the IS were 75.0 mM and +10.9 mV in the first insertion (**Fig. 3Ba**), 70.9 mM and +11.5 mV in the second insertion (**Fig. 3Bb**), and 73.5 mM and +11.8 mV in the third insertion (**Fig. 3Bc**) (*filled circles*). Moreover, in **Fig. 3B**, the measurements of marginal-cells' properties were relatively stable and thereby likely to be successful. During the perfusion, the $a\mathrm{K}^+$ and potential of marginal cells seemed to decrease; these values were 81.6 mM and +91.3 mV in the first insertion (**Fig. 3Ba**), 63.1 mM and +32.1 mV in the second insertion (**Fig. 3Bb**), and 41.7 mM and +21.1 mV in the third insertion (**Fig. 3Bc**). In contrast, the perilymphatic perfusion of ouabain (50 µM) had significant effects on the syncytium (**Fig. 3C**). This perturbation markedly decreased $a\mathrm{K}^+_{\mathrm{Syn}}$ as well as moderately hyperpolarized $\mathrm{V}_{\mathrm{Syn}}$ (**Figs. 3Ca**, **3Cb** and **3Cc**). These results resemble our previous findings [1] and confirm that the syncytial $\mathrm{Na}^+,\mathrm{K}^+$-ATPases actively uptake K^+ to maintain high $a\mathrm{K}^+_{\mathrm{Syn}}$. This local K^+ transport must be required for the unidirectional K^+ transport through the lateral wall. Additionally, in the example of **Fig. 3C**, it seemed probable that, during the perfusion, the marginal-cells' potential was gradually reduced in a similar manner to the EP (see **Fig. 2C**) whereas their $a\mathrm{K}^+$ remained almost unchanged (80-90 mM).

We further statistically compared the syncytial properties recorded in five different conditions; under the normal condition (11 cochleae), during perilymphatic perfusion of the control solution (22 cochleae), that of bumetanide (12 cochleae), that of ouabain (6 cochleae), and under vascular injection of bumetanide (6 cochleae) (**Fig. 3D**). Among the latter four conditions, only the data during the perfusion of ouabain significantly differ from those under the normal

condition (Tukey-Kramer, $p<0.0001$ for $a\mathrm{K^+_{Syn}}$ and $p<0.0001$ for $\mathrm{V_{Syn}}$), as previously reported [1]. Notably, the syncytial properties measured during the perilymphatic perfusion of bumetanide failed to show a significant difference from those under the normal condition (Tukey-Kramer, $p=0.9996$ for $a\mathrm{K^+_{Syn}}$ and $p=0.4427$ for $\mathrm{V_{Syn}}$).

Taken together, the syncytial properties seem to be unaffected during the perilymphatic perfusion of bumetanide (**Fig. 3D**); on the basis of **Eq. 1**, the suppression of the ISP under this condition may be attributable to the increase of $a\mathrm{K^+_{IS}}$ (**Fig. 2A**). We finally intended to prove this hypothesis (**Fig. 4**). Again, the ISP primarily represents the sum of $\mathrm{V_{Syn}}$ and the $\mathrm{K^+}$ diffusion potential across the apical surface of the syncytium (**Eq. 1**). This is obvious when we evaluated the experimental results during the perilymphatic perfusion of the control solution as well as imposition of anoxia (in **Fig. 2A**); the ISP calculated by **Eq. 1** with the recorded $a\mathrm{K^+_{IS}}$, $\mathrm{V_{Syn}}$, and $a\mathrm{K^+_{Syn}}$ corresponded to the measured ISP (**Fig. 4Ab** and **4Bb**), as we reported previously [27]. As shown in **Figs. 2**, **3**, and **5**, during the perilymphatic perfusion of bumetanide the $a\mathrm{K^+_{IS}}$ increased and the ISP decreased but the $a\mathrm{K^+_{Syn}}$ and $\mathrm{V_{Syn}}$ were likely to remain constant. On the assumption that the syncytial properties were unchanged, we predicted the ISP by **Eq. 1** with measured values of $a\mathrm{K^+_{Syn}}$, $\mathrm{V_{Syn}}$, and $a\mathrm{K^+_{IS}}$ (see **Fig. 2A**) and compared it with the recorded ISP (**Fig. 4A**). While $a\mathrm{K^+_{IS}}$ remained almost unchanged, the predicted ISP exceeded the measured ISP, by ~20 mV at maximum. This difference gradually diminished as the $a\mathrm{K^+_{IS}}$ increased. In 15 min, the two ISPs corresponded with each other. These observations verify the above assumption and also demonstrate that the ISP reduction stems primarily from modulation of the $\mathrm{K^+}$ diffusion potential across the apical surface of the syncytium although in the initial phase it may involve different factors (see **Discussion**).

During the perilymphatic perfusion of ouabain as well, the ISP reduction primarily depends on the modulation of the $\mathrm{K^+}$ diffusion potential, because $\mathrm{V_{Syn}}$ hyperpolarizes only moderately (**Figs. 2C**, **3C**, **3D**, and **5**; see **Eq. 1**) [1]. In this condition, the $a\mathrm{K^+_{Syn}}$ greatly decreases but $a\mathrm{K^+_{IS}}$ remains nearly constant, indicating that the mechanism underlying the ISP reduction differs from that during the perfusion of bumetanide. In support of this, the ISP predicted with the measured $a\mathrm{K^+_{IS}}$ on the assumption that $a\mathrm{K^+_{Syn}}$ and $\mathrm{V_{Syn}}$ were constant never matched with the measured ISP (**Fig. 4B**).

If the syncytial NKCCs would also contribute to the $\mathrm{K^+}$ transport, then inhibition of the transporters should decrease $a\mathrm{K^+_{Syn}}$ in a manner similar to that of the $\mathrm{Na^+,K^+}$-ATPases. However, this was not the case (**Figs. 3** and **4**). Therefore, contrary to the marginal-cells' NKCCs, the NKCCs on the basolateral surface of the syncytium would negligibly uptake $\mathrm{K^+}$ and thus be "silent" on driving the unidirectional $\mathrm{K^+}$ transport. The effects on the electrochemical properties of the lateral wall of the perilymphatically perfused bumetanide were similar to those of the vascularly injected bumetanide (**Figs. 2A**, **2B** and **3D**). This result implies that the former reaches the basolateral surface of marginal cells and inhibits their NKCCs.

Discussion

The syncytial NKCCs may be silent on the unidirectional K^+ transport across the lateral wall

The unidirectional K^+ transport through the lateral wall plays central roles in maintaining the EP and perhaps endolymphatic high $[K^+]$ [11, 25]. Because these properties are essential for cochlear function, analyses of the mechanisms underlying the establishment of the K^+ transport are of importance to understand signal transduction networks in the hearing system and clarify the pathophysiological processes of deafness. Out of the four membrane domains forming the two functional layers of the lateral wall (**Fig. 1B**), ion-transport mechanisms on the basolateral surface of the marginal cells have been well characterized. On this domain, the NKCCs and the Na^+,K^+-ATPases occur together and seem to be functionally coupled to drive the unidirectional K^+ transport [27, 28]. In support of this, inhibition of either the transporters or the pumps causes aK^+_{IS} to increase and aK^+_{MC} to decrease [27] (**Figs. 2B** and **5**). On the basolateral surface of the syncytium, the elements involved in the K^+ transport remains largely uncertain, although the crucial role of the Na^+,K^+-ATPases has been demonstrated [1]. A major reason might be that patch-clamp analyses of the fibrocytes are technically difficult, owed to complicated morphology of the cell membranes and excess amount of extracellular matrix [16]. Therefore, *in vivo* experiments with double-barreled ion-selective electrode are effective and are currently the sole procedures to investigate the physiological ion-transport through the basolateral surface of the syncytium.

Classical electrophysiological assays and various histological experiments imply that the functional NKCCs occur on the fibrocytes' plasma membrane (see first paragraph in "**Results**"). Our earlier study with K^+-selective electrodes demonstrated that the syncytial Na^+,K^+-ATPases, which are coexpressed with the NKCCs, actually uptake K^+ and play pivotal roles in maintenance of high aK^+_{Syn} [1] (**Fig. 3C**). In accordance with these observations as well as on the analogy of the K^+ transport system across the marginal-cells' basolateral surface, it is reasonable to assume that the NKCCs on the basolateral surface of the syncytium participate in the unidirectional K^+ transport through the lateral wall and thereby contribute to establishment of the EP [10, 25, 49, 52]. However, our findings contradict this assumption (**Figs. 2** and **3**). We conclude that, on the basolateral surface of the syncytial layer the Na^+,K^+-ATPases would dominate in the pathway for the K^+ transport whereas on the basolateral surface of the marginal-cell layer both the NKCCs and Na^+,K^+-ATPases are involved in it (**Fig. 5**).

Roles of "silent" NKCCs in the syncytium of the lateral cochlear wall remain elusive but they could be involved in ion homeostasis of the extracellular fluid as suggested in NKCCs of the choroid plexus epithelium (for a review, see Damkier et al [6]). This epithelium also coexpresses type-1 NKCCs and Na^+,K^+-ATPases on the surface exposed to the cerebrospinal fluid (CSF), which is connected with the perilymph. The Na^+,K^+-ATPases actively uptake K^+ from the CSF. Like the syncytium [15], under physiological conditions the choroid plexus epithelium exhibits unusually high

intracellular [Na$^+$] and [Cl$^-$] and low intracellular [K$^+$], as compared with common tissue types. This arrangement in the epithelium significantly attenuates the concentration gradient of each ion across the membrane and therefore provides the NKCCs with little driving force for ion-transport. In other words, the NKCCs are "silent" and the Na$^+$,K$^+$-ATPases govern the K$^+$ transport from the CSF into the epithelium under physiological conditions. Previous experiments demonstrated that significant augmentation of extracellular [K$^+$] modulated the driving force and permitted the NKCCs to import [K$^+$] [51]. This regulatory system could operate by pathophysiological events such as cell injury in order to keep the CSF's [K$^+$] constant. On the analogy to the choroid plexus epithelium, the syncytial NKCCs may be silent under physiological conditions due to the unique intracellular ionic properties (see above) and they could also serve the similar feedback mechanism in particular cases to control the perilymphatic [K$^+$] in the microenvironment surrounding the cochlear fibrocytes. Because intracellular [Na$^+$] of the marginal cells is as low as that of common cell types [15], the large concentration gradient of Na$^+$ occurs across the basolateral surface and it drives NKCCs to actively import K$^+$ even under physiological conditions.

Mechanism underlying the reduction of the EP

Our experiments further indicate the possible processes by which the EP was reduced during the perilymphatic perfusion of bumetanide. Under this condition, the ISP always exceeded the EP (**Figs. 2A** and **3B**). The potential difference, which occurs across the marginal-cell layer, might be significantly involved in the reduction of the EP. The similar potential difference was detected when the Na$^+$,K$^+$-ATPases or the NKCCs on the basolateral surface of the marginal-cell layer were blocked by anoxia or by the vascularly perfused blockers (**Fig. 2B**) [1, 27]. We previously identified that, during anoxia, the potential difference resulted primarily from the altered membrane potential across the apical surfaces of the marginal cells and the ISP was nearly equal to the potential inside the marginal cells relative to the perilymph (**Fig. 5**). Furthermore, aK$^+$ inside the marginal cells (aK$^+_{MC}$) dramatically decreased whereas aK$^+$ in the endolymph (aK$^+_{EL}$) remained constant [1, 27]. On the apical membranes of the marginal cells, the K$^+$ permeability, which mainly stems from I$_{Ks}$ K$^+$ channels (**Fig. 1B**) [8, 34], significantly exceeds the Na$^+$ and Cl$^-$ permeabilities [42]. These observations imply that the potential difference across the marginal-cell layer emerges from a K$^+$ diffusion potential and the EP represents the sum of the diffusion potential and the ISP [11, 27]:

$$\mathrm{EP} \approx \mathrm{ISP} + \frac{RT}{F} \cdot \ln\left(\frac{a\mathrm{K}^+_{MC}}{a\mathrm{K}^+_{EL}}\right).$$

Eq. 2

In support of this formulation, the measured EP closely matched the EP predicted by **Eq. 2** during anoxia, using measured values of the potential of the marginal cells (equal to the ISP; see above), aK$^+_{MC}$ and aK$^+_{EL}$ [11, 27]. Similarly, the aK$^+_{MC}$ greatly decreases during the vascular injection of bumetanide [11, 27] and also this is likely to be the case during its

perilymphatic perfusion (**Figs. 3B** and **5**). Therefore, in the latter condition the EP reduction depends not only on the modulation of the ISP (**Fig. 2A** and **Eq. 1**) but also on the modulation of the K^+ diffusion potential across the apical membranes of the marginal cells (**Eq. 2** and **Fig. 5**). When the blocker markedly causes the ISP to decrease and the K^+ diffusion potential to enlarge, the EP reaches a negative value (**Figs. 2A** and **5**).

The suppression of the EP by blocking the syncytial Na^+,K^+-ATPases is attributed to a different mechanism. During the perilymphatic perfusion of ouabain, the potential difference across the marginal-cell layer remains unchanged and is small (~6 mV; **Figs. 2C** and **3C**). It indicates that the change of the EP depends on the ISP reduction that emerges primarily from the $aK^+{}_{Syn}$ decrease (**Eqs. 1** and **2**; **Figs. 4** and **5**) and the blocker affects the pumps on the basolateral surface of the syncytium but does not reach those of the marginal cells [1]. Our experiment showed that the minimum ISP during the perfusion of ouabain was a positive value of +12 mV (**Fig. 2C**). Therefore, the EP reduced to approximately 0 mV when ouabain sufficiently blocked the Na^+,K^+-ATPases.

Of note, aforementioned **Eqs. 1** and **2** contain a few approximations. It seems probable that, *in vivo*, the K^+ transport through the lateral wall links with K^+ flow across the hair-cell's layer and thereby K^+ is unidirectionally "circulated" between these two components [7, 18]. This circulation current would continuously flow throughout the cochlea even without acoustic stimulation [7]. On the basis of this idea as well as of the Hodgkin-Huxley model, we previously developed an equivalent circuit model that incorporated the channels and transporters involved in the circulation current in order to simulate the electrochemical properties of the extra/intracellular fluids of the lateral wall and the endolymph under various conditions [28]. In accordance with the principles of the model, the ISP, which is the sum of V_{Syn} and the membrane potentials of the apical surface of the syncytium, under normal conditions can be described by

$$ISP = V_{Syn} + \frac{g_{Na,IC} \cdot E_{Na,IC} + g_{K,IC} \cdot E_{K,IC} + g_{Cl,IC} \cdot E_{Cl,IC} + I_{Cir}}{g_{Na,IC} + g_{K,IC} + g_{Cl,IC}}, \quad \textbf{Eq. 3}$$

where $g_{Na,IC}$, $g_{K,IC}$ and $g_{Cl,IC}$ are conductances of Na^+, K^+ and Cl^- on the intermediate-cells' membranes that provide the apical surface of the syncytium, $E_{Na,IC}$, $E_{K,IC}$, $E_{Cl,IC}$ are the diffusion potentials or alternatively termed the equilibrium potentials of Na^+, K^+ and Cl^- on the intermediate-cells' membranes, and I_{Cir} is the circulation current.

Since K^+ permeability dominates the apical surface of the syncytium [43], the conductances of Na^+ and Cl^- can be neglected from **Eq. 3**:

$$ISP \approx V_{Syn} + \frac{RT}{F} \cdot \ln\left(\frac{aK^+{}_{Syn}}{aK^+{}_{IS}}\right) + \frac{I_{Cir}}{g_{K,IC}}. \quad \textbf{Eq. 4}$$

In this equation, the third term on the right side corresponds to the transmembrane voltage drop that is yielded by the constant flow of the circulation current. Under normal conditions this voltage drop might be negligible because the ISP

predicted with the measured V_{Syn}, aK^+_{Syn} and aK^+_{IS} by **Eq. 1** that comprises the first and second terms on the right side of **Eq. 4** matched well with the recorded ISP during the perfusion of the control solution (**Fig. 4**). Indeed, with I_{Cir} and $g_{K,IC}$ that are estimated from the measured current across the isolated hair cells and intermediate cells [17, 44], the transmembrane voltage drop is calculated to be roughly 2 mV, which is much less than the amplitude of the diffusion potential of K$^+$ (~80 mV; **Eq. 4**) [28]. Accordingly, it is reasonable to omit the transmembrane voltage drop for simplicity as described in **Eq. 1**. These approximations can be also applied to the apical surface of marginal cells (**Eq. 2**) [27, 28].

Eq. 1 was valid during anoxia and when the change of IS's properties by perilymphatically perfused bumetanide was being saturated (**Fig. 4Ab**). On the other hand, in the initial phase of the perfusion, the ISP predicted by **Eq. 1** significantly exceeded the measured ISP (**Fig. 4Ab**). The mechanism underlying the difference remains uncertain but might be owed to the possibility that $g_{Na,IC}$, $g_{K,IC}$, $g_{Cl,IC}$, and/or even I_{Cir} were transiently affected when bumetanide was crossing the syncytium and/or by other factors (**Eq. 3**).

Ion-transport profile on the basolateral surface of the syncytium

In the marginal cells, the Cl$^-$ channels comprising ClC-K and barttin subunits occur together with NKCCs on the basolateral surfaces and locally recycle the Cl$^-$ taken up by the transporters [8, 33] (**Fig. 1B**). Qu et al [30, 31] detected the immunolabeling of the ClC-K in the type II, IV and V fibrocytes and also measured Cl$^-$ currents in cultured cells. They therefore proposed that, on the basolateral surface of the syncytium, the ClC-K/barttin channels could play similar roles in the Cl$^-$ recycling. However, this is currently controversial because the immunolabeling of neither ClC-K nor barttin has been observed in other studies [8, 32, 33]. Under physiological conditions, V_{Syn} is slightly depolarized relative to the perilymph (**Figs. 3A** and **3D**), and [Cl$^-$] in the perilymph exceeds that inside the syncytium [15, 28]. The electrochemical gradient elicited by these milieus is expected to cause the influx of Cl$^-$ from the perilymph to the syncytium through the channels, even if they would exist in the syncytium. This direction of the Cl$^-$-flux is inconsistent with that in the aforementioned proposal. Because the syncytial NKCCs are unlikely to transport K$^+$ (**Figs. 3** and **5**), they may be silent on uptake of Cl$^-$ as well. In this case, the basolateral surface of the syncytium could require neither the Cl$^-$-recycling system nor the Cl$^-$ conductance. It might be important to prove these hypotheses.

Possible routes of bumetanide transport across the syncytium

Our present study implies that the perilymphatically applied bumetanide crosses the syncytial layer, reaches the IS, and affects the NKCCs on the basolateral membranes of the marginal cells. It might explain that the time-course of the change of IS's properties by the perilymphatic perfusion was significantly slower than that by the vascular injection (**Figs. 2A** and **2B**). The above implication is supported by following observations. Vascular injection of bumetanide enlarges the

IS, indicating that ion-transport of the marginal-cells' NKCCs significantly contributes to the water homeostasis in the stria vascularis [36]. Higashiyama et al [12] found that the perilymphatically perfused bumetanide had a similar effect on the IS. Based on this, they claimed that the major action site of bumetanide would be the basolateral membranes of the marginal cells.

It remains uncertain how bumetanide reaches the IS, but there are a few possibilities. First, this reagent is lipophilic and therefore it could considerably permeate the membranes of the cells constituting the syncytium, as discussed in Higashiyama et al [12]. Second possibility is an involvement of the membrane transport mechanisms such as the organic anion transporters (OATs). Indeed, in the renal proximal tubules, these apparatus transport the vascularly applied bumetanide to the apical surface of the epithelial cells [37]. It is of interest to determine the pathway for bumetanide in the lateral wall.

Acknowledgments

Conflict of interest

None.

Ethical standards

The experiments comply with the current laws of Japan.

References

1. Adachi N, Yoshida T, Nin F, Ogata G, Yamaguchi S, Suzuki T, Komune S, Hisa Y, Hibino H, Kurachi Y (2013) The mechanism underlying maintenance of the endocochlear potential by the K^+ transport system in fibrocytes of the inner ear. J Physiol 591:4459-4472 DOI: 10.1113/jphysiol.2013.258046

2. Ando M, Takeuchi S (1999) Immunological identification of an inward rectifier K^+ channel (Kir4.1) in the intermediate cell (melanocyte) of the cochlear stria vascularis of gerbils and rats. Cell Tissue Res 298:179-183 DOI: 10.1007/s004419900066

3. Békésy G (1952) DC Resting Potentials Inside the Cochlear Partition. J Acoust Soc Am 24:72 DOI: 10.1121/1.1906851

4. Brown KT, Crawford JM (1967) Intracellular recording of rapid light-evoked responses from pigment epithelium cells of the frog eye. Vision Res 7:149-163 DOI: 10.1016/0042-6989(67)90080-6

5. Crouch JJ, Sakaguchi N, Lytle C, Schulte BA (1997) Immunohistochemical localization of the Na-K-Cl co-transporter (NKCC1) in the gerbil inner ear. J Histochem Cytochem 45:773-778 DOI: 10.1177/002215549704500601

6. Damkier HH, Brown PD, Praetorius J (2010) Epithelial Pathways in Choroid Plexus Electrolyte Transport. Physiology (Bethesda) 25:239-249 DOI: 10.1152/physiol.00011.2010

7. Davis H (1961) Some principles of sensory receptor action. Physiol Rev 41:391-416 PMID: 13720173

8. Estevez R, Boettger T, Stein V, Birkenhager R, Otto E, Hildebrandt F, Jentsch TJ (2001) Barttin is a Cl- channel beta-subunit crucial for renal Cl- reabsorption and inner ear K^+ secretion. Nature 414:558-561 DOI: 10.1038/35107099

9. Flagella M, Clarke LL, Miller ML, Erway LC, Giannella RA, Andringa A, Gawenis LR, Kramer J, Duffy JJ, Doetschman T, Lorenz JN, Yamoah EN, Cardell EL, Shull GE (1999) Mice lacking the basolateral Na-K-2Cl cotransporter have impaired epithelial chloride secretion and are profoundly deaf. J Biol Chem 274:26946-26955 DOI: 10.1074/jbc.274.38.26946

10. Hibino H, Kurachi Y (2006) Molecular and physiological bases of the K^+ circulation in the mammalian inner ear. Physiology (Bethesda) 21:336-345 DOI: 10.1152/physiol.00023.2006

11. Hibino H, Nin F, Tsuzuki C, Kurachi Y (2010) How is the highly positive endocochlear potential formed? The specific architecture of the stria vascularis and the roles of the ion-transport apparatus. Pflugers Arch 459:521-533 DOI: 10.1007/s00424-009-0754-z

12. Higashiyama K, Takeuchi S, Azuma H, Sawada S, Yamakawa K, Kakigi A, Takeda T (2003) Bumetanide-induced enlargement of the intercellular space in the stria vascularis critically depends on Na^+ transport. Hear Res 186:1-9 DOI: 10.1016/s0378-5955(03)00226-0

13. Hinojosa R, Rodriguez-Echandia EL (1966) The fine structure of the stria vascularis of the cat inner ear. Am J Anat 118:631-663 DOI: 10.1002/aja.1001180218

14. Hudspeth AJ (1989) How the ear's works work. Nature 341:397-404 DOI: 10.1038/341397a0

15. Ikeda K, Morizono T (1989) Electrochemical profiles for monovalent ions in the stria vascularis: cellular model of ion transport mechanisms. Hear Res 39:279-286 DOI: 10.1016/0378-5955(89)90047-6

16. Kelly JJ, Forge A, Jagger DJ (2012) Contractility in type III cochlear fibrocytes is dependent on non-muscle myosin

II and intercellular gap junctional coupling. J Assoc Res Otolaryngol 13:473-484 DOI: 10.1007/s10162-012-0322-7

17. Kennedy HJ, Evans MG, Crawford AC, Fettiplace R (2003) Fast adaptation of mechanoelectrical transducer channels in mammalian cochlear hair cells. Nat Neurosci 6:832-836 DOI: 10.1038/nn1089

18. Kikuchi T, Adams JC, Miyabe Y, So E, Kobayashi T (2000) Potassium ion recycling pathway via gap junction systems in the mammalian cochlea and its interruption in hereditary nonsyndromic deafness. Med Electron Microsc 33:51-56 DOI: 10.1007/s007950000009

19. Kikuchi T, Kimura RS, Paul DL, Adams JC (1995) Gap junctions in the rat cochlea: immunohistochemical and ultrastructural analysis. Anat Embryol (Berl) 191:101-118 DOI: 10.1007/BF00186783

20. Konishi T, Butler RA, Fernandez C (1961) Effect of anoxia on cochlear potentials. J Acoust Soc Am 33:349-356 DOI: 10.1121/1.1908659

21. Konishi T, Salt AN (1983) Electrochemical profile for potassium ions across the cochlear hair cell membranes of normal and noise-exposed guinea pigs. Hear Res 11:219-233 DOI: 10.1016/0378-5955(83)90080-1

22. Kuijpers W, Bonting SL (1970) The cochlear potentials. II. The nature of the cochlear endolymphatic resting potential. Pflugers Arch 320:359-372 DOI: 10.1007/BF00588214

23. Kusakari J, Ise I, Comegys TH, Thalmann I, Thalmann R (1978) Effect of ethacrynic acid, furosemide, and ouabain upon the endolymphatic potential and upon high energy phosphates of the stria vascularis. Laryngoscope 88:12-37 DOI: PMID: 619186

24. Kusakari J, Kambayashi J, Ise I, Kawamoto K (1978) Reduction of the endocochlear potential by the new "loop" diuretic, bumetanide. Acta Otolaryngol 86:336-341 DOI: 10.3109/00016487809124755

25. Marcus DC, Wangemann P (2010) Inner ear fluid homeostasis. In: Moore DR (ed) The Oxford handbook of auditory science - the ear. Oxford University Press, Oxford, pp. 213-230

26. Mizuta K, Adachi M, Iwasa KH (1997) Ultrastructural localization of the Na-K-Cl cotransporter in the lateral wall of the rabbit cochlear duct. Hear Res 106:154-162 DOI: 10.1016/S0378-5955(97)00010-5

27. Nin F, Hibino H, Doi K, Suzuki T, Hisa Y, Kurachi Y (2008) The endocochlear potential depends on two K^+ diffusion potentials and an electrical barrier in the stria vascularis of the inner ear. Proc Natl Acad Sci U S A 105:1751-1756 DOI: 10.1073/pnas.0711463105

28. Nin F, Hibino H, Murakami S, Suzuki T, Hisa Y, Kurachi Y (2012) Computational model of a circulation current that controls electrochemical properties in the mammalian cochlea. Proc Natl Acad Sci U S A 109:9191-9196 DOI: 10.1073/pnas.1120067109

29. Pace AJ, Madden VJ, Henson OW, Jr., Koller BH, Henson MM (2001) Ultrastructure of the inner ear of NKCC1-deficient mice. Hear Res 156:17-30 DOI: 10.1016/S0378-5955(01)00263-5

30. Qu C, Liang F, Hu W, Shen Z, Spicer SS, Schulte BA (2006) Expression of CLC-K chloride channels in the rat cochlea. Hear Res 213:79-87 DOI: 10.1016/j.heares.2005.12.012

31. Qu C, Liang F, Smythe NM, Schulte BA (2007) Identification of ClC-2 and CIC-K2 chloride channels in cultured rat type IV spiral ligament fibrocytes. J Assoc Res Otolaryngol 8:205-219 DOI: 10.1007/s10162-007-0072-0

32. Rickheit G, Maier H, Strenzke N, Andreescu CE, De Zeeuw CI, Muenscher A, Zdebik AA, Jentsch TJ (2008)

Endocochlear potential depends on Cl⁻ channels: mechanism underlying deafness in Bartter syndrome IV. EMBO J 27:2907-2917 DOI: 10.1038/emboj.2008.203

33. Sage CL, Marcus DC (2001) Immunolocalization of ClC-K chloride channel in strial marginal cells and vestibular dark cells. Hear Res 160:1-9 DOI: 10.1016/S0378-5955(01)00308-2

34. Sakagami M, Fukazawa K, Matsunaga T, Fujita H, Mori N, Takumi T, Ohkubo H, Nakanishi S (1991) Cellular localization of rat I_{sk} protein in the stria vascularis by immunohistochemical observation. Hear Res 56:168-172 DOI: 10.1016/0378-5955(91)90166-7

35. Salt AN, Melichar I, Thalmann R (1987) Mechanisms of endocochlear potential generation by stria vascularis. Laryngoscope 97:984-991 DOI: 10.1288/00005537-198708000-00020

36. Santi PA, Duvall AJ, 3rd (1979) Morphological alteration of the stria vascularis after administration of the diuretic bumetanide. Acta Otolaryngol 88:1-12 DOI: 10.3109/00016487909137133

37. Sekine T, Miyazaki H, Endou H (2006) Molecular physiology of renal organic anion transporters. Am J Physiol Renal Physiol 290:F251-261 DOI: 10.1152/ajprenal.00439.2004

38. Shen W, Purpura LA, Li B, Nan C, Chang IJ, Ripps H (2013) Regulation of synaptic transmission at the photoreceptor terminal: a novel role for the cation-chloride co-transporter NKCC1. J Physiol 591:133-147 DOI: 10.1113/jphysiol.2012.241042

39. Slepecky NB (1996) Cochlear Structure. In: Dallos P, Popper AN, Fay RR (eds) The cochlea. Springer New York, pp. 44-129

40. Spicer SS, Schulte BA (1996) The fine structure of spiral ligament cells relates to ion return to the stria and varies with place-frequency. Hear Res 100:80-100 DOI: 10.1016/0378-5955(96)00106-2

41 Spicer SS, Schulte BA (2005) Novel structures in marginal and intermediate cells presumably relate to functions of apical versus basal strial strata. Hear Res 200:87-101 DOI: 10.1016/j.heares.2004.09.006

42 Sunose H, Ikeda K, Suzuki M, Takasaka T (1994) Voltage-activated K channel in luminal membrane of marginal cells of stria vascularis dissected from guinea pig. Hear Res 80:86-92 DOI: 10.1016/0378-5955(94)90012-4

43. Takeuchi S, Ando M (1998) Inwardly rectifying K⁺ currents in intermediate cells in the cochlea of gerbils: a possible contribution to the endocochlear potential. Neurosci Lett 247:175-178 DOI: 10.1016/S0304-3940(98)00318-8

44. Takeuchi S, Ando M (1999) Voltage-dependent outward K⁺ current in intermediate cell of stria vascularis of gerbil cochlea. Am J Physiol 277:C91-99 PMID: 10409112

45. Takeuchi S, Ando M, Kakigi A (2000) Mechanism generating endocochlear potential: role played by intermediate cells in stria vascularis. Biophys J 79:2572-2582 DOI: 10.1016/S0006-3495(00)76497-6

46. Wada J, Paloheimo S, Thalmann I, Bohne BA, Thalmann R (1979) Maintenance of cochlear function with artificial oxygen carriers. Laryngoscope 89:1457-1473 DOI: 10.1002/lary.5540890911

47. Wangemann P (2006) Supporting sensory transduction: cochlear fluid homeostasis and the endocochlear potential. J Physiol 576:11-21 DOI: 10.1113/jphysiol.2006.112888

48. Wangemann P, Liu J, Marcus DC (1995) Ion transport mechanisms responsible for K⁺ secretion and the transepithelial voltage across marginal cells of stria vascularis in vitro. Hear Res 84:19-29 DOI: 10.1016/0378-5955(95)00009-S

49. Weber PC, Cunningham CD, 3rd, Schulte BA (2001) Potassium recycling pathways in the human cochlea. Laryngoscope 111:1156-1165 DOI: 10.1097/00005537-200107000-00006

50. Wu MF, Pang ZP, Zhuo M, Xu ZC (2005) Prolonged membrane potential depolarization in cingulate pyramidal cells after digit amputation in adult rats. Mol Pain 1:23 DOI: 10.1186/1744-8069-1-23

51. Wu Q, Delpire E, Hebert SC, Strange K (1998) Functional demonstration of Na^+-K^+-$2Cl^-$ cotransporter activity in isolated, polarized choroid plexus cells. Am J Physiol 275:C1565-1572 PMID: 9843718

52. Zdebik AA, Wangemann P, Jentsch TJ (2009) Potassium ion movement in the inner ear: insights from genetic disease and mouse models. Physiology (Bethesda) 24:307-316 DOI: 10.1152/physiol.00018.2009

Figure legends

Fig. 1 Structure and electrochemical properties of the cochlea and its lateral wall

A; The ionic composition and potential of the endolymph are considered to be maintained by the unidirectional K^+ transport thorough the lateral cochlear wall (*red arrow* on the left). This transport seems to be linked with the K^+ flow through the hair cells (*red arrow* in the center). The location of five types of the fibrocytes is indicated by *roman* numbers.

B; *Top* illustrates extracellular and intracellular compartments of the lateral wall and ion-transport apparatus involved in the unidirectional K^+ transport. Of note, the lateral wall is made up of two functional epithelial layers (see ***Introduction***) and thereby contains four membrane domains, apical (api) and basolateral (baso) surfaces of the syncytial and marginal-cell layers. *Bottom* shows the profile of the electrochemical properties of the lateral wall under physiological conditions. Each compartment is characterized by different combination of aK^+ (*blue*) and potential (*red*). NKCC, $Na^+,K^+,2Cl^-$-cotransporter; ClC, ClC-K/barttin Cl^- channels; TJ, tight junction; MC, marginal cell; IC, intermediate cell; BC, basal cell; ISP, intrastrial potential; EP, endocochlear potential. *A* and *B* are modified from **Fig. 1** in Nin et al [27]

Fig. 2 Properties of the IS during application of blockers for K^+ transport apparatus

The aK^+ (*blue*) and potential (*red*) of compartments of the lateral cochlear wall were recorded with a double-barreled K^+ selective electrode advanced from the perilymphatic space (PL; *open bars* above the traces) to the endolymph (*blue bars* above the traces) (*upper panels* in *A*, *B*, and *C*). In each experiment, the EP (*orange*) was simultaneously monitored by a single-barreled electrode located in the endolymph (*lower panels* in *A*, *B*, and *C*). In this and subsequent recordings (see **Figs. 3** and **4**), *open* and *filled wedges* at the top of each panel indicate the periods during which the electrode was inserted towards the endolymph and withdrawn to the perilymph, respectively.

A; The effect of the perilymphatic perfusion of bumetanide. In this experiment, the control solution was first perfused for ~30 min. Then, while the solution continued to be applied, the K^+-selective electrode was driven across the lateral wall. Before entering the IS, we detected a region of the syncytial layer (*black bars* above the traces). While the electrode was held in the intrastrial space (IS) (*green bars* above the traces), the animal was imposed to anoxia. After reoxygenation, the perfusate was switched to the solution containing bumetanide (100 µM). The electrode was further inserted into the endolymph, which was signaled by a rapid and prominent elevation of aK^+, and finally retracted into the perilymphatic space. The area surrounded by *square* and *broken square* in *upper panel* are displayed in **Figs. 4Aa** and **4Ab**, respectively.

B; The effect of vascular injection of bumetanide. While measuring the aK^+ and potential by the K^+-selective electrode located in the IS, the solution containing bumetanide (30 mg/kg; 3 ml) was injected to the right jugular vein in 3 min (iv).

C; The effect of perilymphatic perfusion of ouabain. The experiment was also performed in accordance with the

protocol in **A**. In this case, while the K$^+$-selective electrode was held in the IS, the solution containing ouabain (50 μM) was perfused to the perilymhatic space. The area surrounded by *square* and *broken square* in *upper panel* are displayed in **Figs. 4Ba** and **4Bb**, respectively

Fig. 3 Analyses of the syncytium

A, **B**, *and* **C**; While perfusates were being applied into the perilymphatic space, the K$^+$-selective electrodes were inserted multiple times from the perilymph (PL; *open bars* above the traces) to the endolymph (EL; *blue bars* above the traces) to examine the electrochemical properties of the syncytium (*black bars* above the traces) (***a***, ***b***, and ***c***). The traces of the EP (*orange*), which was simultaneously recorded by a single-barreled electrode placed in the endolymph, were displayed in ***d*** as well as overlaid with the traces of the potentials measured by the K$^+$-selective electrodes (see ***a***, ***b***, and ***c***). Insertions of the K$^+$-selective electrodes were performed during the periods highlighted by *squares* in ***d***. In **A**, we performed the first measurement with a double-barreled K$^+$-selective electrode in the lateral wall treated with no perfusate (***a***). Thereafter, while perilymphatically applying the control solution, we advanced different electrodes twice across the lateral wall (***b*** and ***c***). In **B** and **C**, the perfusates were first the control solution and then switched to the solutions containing bumetanide (100 μM; **B**) or ouabain (50 μM; **C**). *Green bars* above the traces indicate the region that is likely to be the IS. In some measurements, the compartment that probably represents the marginal-cell layer (M) was detected. *Open* and *filled circles* mark to the syncytial compartments whose properties were stably measured (***a***, ***b***, and ***c***; see **Results**). As described in **Results** and Adachi et al [1], the aK$^+$ and potential of the compartment adjacent to the IS probably represents the properties of the syncytium (*filled circles*) and thereby were used to quantitatively characterize the effects of the blockers in **D**.

D; Comparison of the effects of the blockers on the electrochemical properties of the syncytium. For this analysis, used were the values of aK$^+_{Syn}$ and V$_{Syn}$ that were recorded when the EP became stable in each experiment. PL and iv indicate perilymphatic and intravenous application of the blockers, respectively. Bars and error bars in the two panels represent the mean ± S.D. obtained from the measurements under the five conditions; normal (11 cochleae), control PL (22 cochleae), bumetanide PL (12 cochleae), ouabain PL (6 cochleae) and bumetanide iv (6 cochleae) [one-way ANOVA: p<0.0001 for aK$^+_{Syn}$ and p<0.0001 for V$_{Syn}$]. The values of mean ± S.D. are also shown above each bar

Fig. 4 Mechanism underlying the reduction of the ISP by bumetanide

Aa and ***Ba***; These panels show the syncytial electrochemical properties surrounded by *square* in **Figs. 2A** and **2C** with an expanded time scale. The aK$^+$ and potential of the compartment neighboring the IS (*filled circle*) in each panel (V$_{Syn}$ and aK$^+_{Syn}$) were used to calculate the ISP in ***Ab*** and ***Bb*** on the assumption that these values were constant

throughout the perilymphatic perfusion of bumetanide (*A*) or ouabain (*B*) (see below).

Ab and *Bb*; The ISP during anoxia and the perfusion of bumetanide (*Ab*) and that of ouabain (*Bb*) (the area surrounded by *broken square* in **Figs. 2A** and **2C**) was predicted (*green*) with the equation, $ISP \approx V_{Syn} + (RT/F) \ln(aK^+_{Syn}/aK^+_{IS})$. The aK^+_{IS} (*blue*) was derived from the data surrounded by *broken square* in **Figs. 2A** and **2C**. The ISP recorded in **Figs. 2A** and **2C** is also displayed (*red*). Syn, syncytium; PL, perilymph; IS, intrastrial space

Fig. 5 Model for the unidirectional K$^+$ transport through the lateral wall

Displayed in *top panel* are the K$^+$ transport apparatus significantly involved in the unidirectional K$^+$ transport. Based on our findings, it seems probable that the NKCCs on the basolateral surface of the syncytium barely contribute to the K$^+$ transport under normal condition and therefore the transporters are omitted in the revised model (see also **Fig. 1B**). The *second*, *third*, and *fourth* panels show the predicted potential and aK^+ in each compartment under the normal condition, during the perilymphatic perfusion (PL) of 100 µM bumetanide, or 50 µM ouabain, respectively. In addition, the effects of intravenous injection (iv) of bumetanide on the lateral wall were summarized in the *bottom panel*. *Arrowheads* filled with *yellow* mark the membrane domains in which a K$^+$ diffusion potential occurs. *Upward* and *downward arrows* show increases and decreases of aK^+ as compared to those under the normal condition. As described in ***Results***, the profile during the perilymphatically applied bumetanide (*third panel*) is similar to that induced by intravenous injection of bumetanide (*bottom panel*). NKCC, Na$^+$,K$^+$,2Cl$^-$-cotransporter; ISP, intrastrial potential; EP, endocochlear potential; api, apical; baso, basolateral. *Top panel* modified from **Fig. 1** in Nin et al [27]
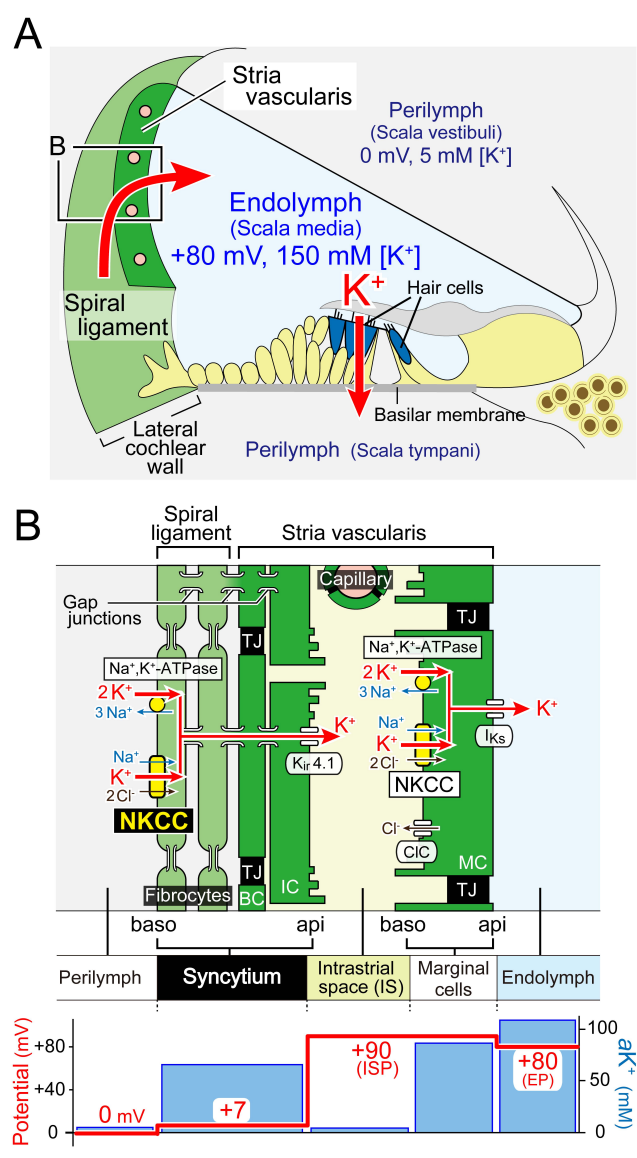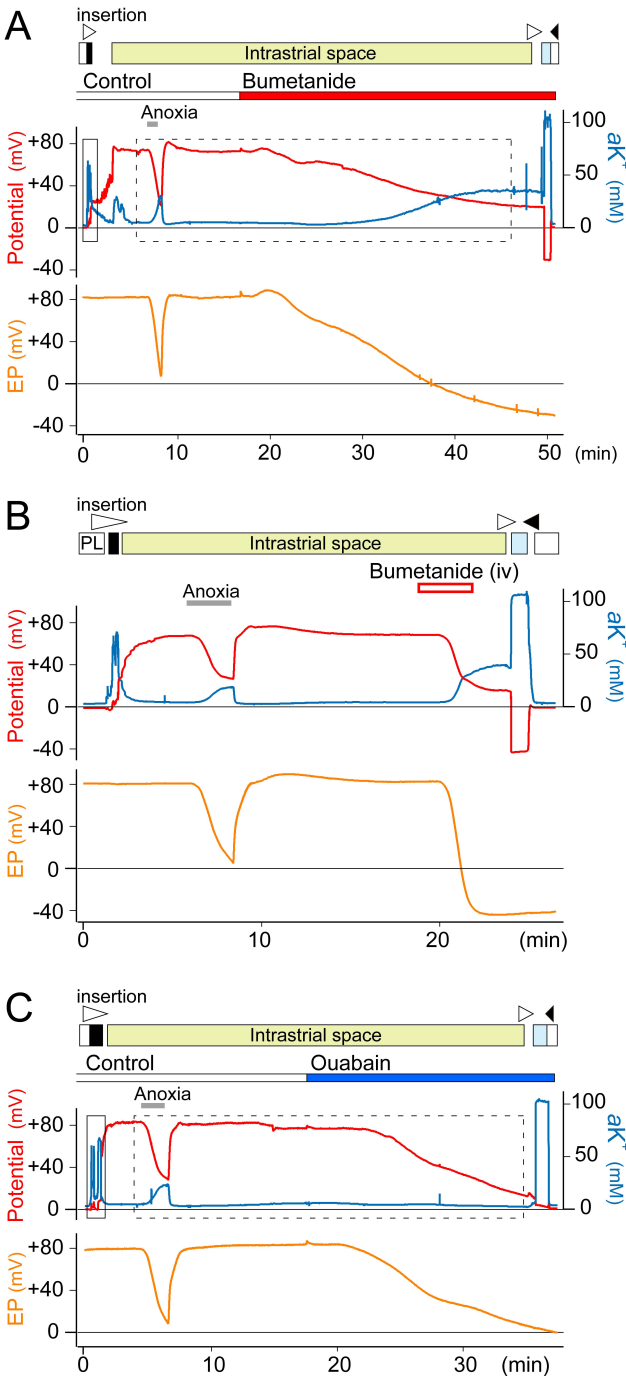
Fig. 1

A

Stria
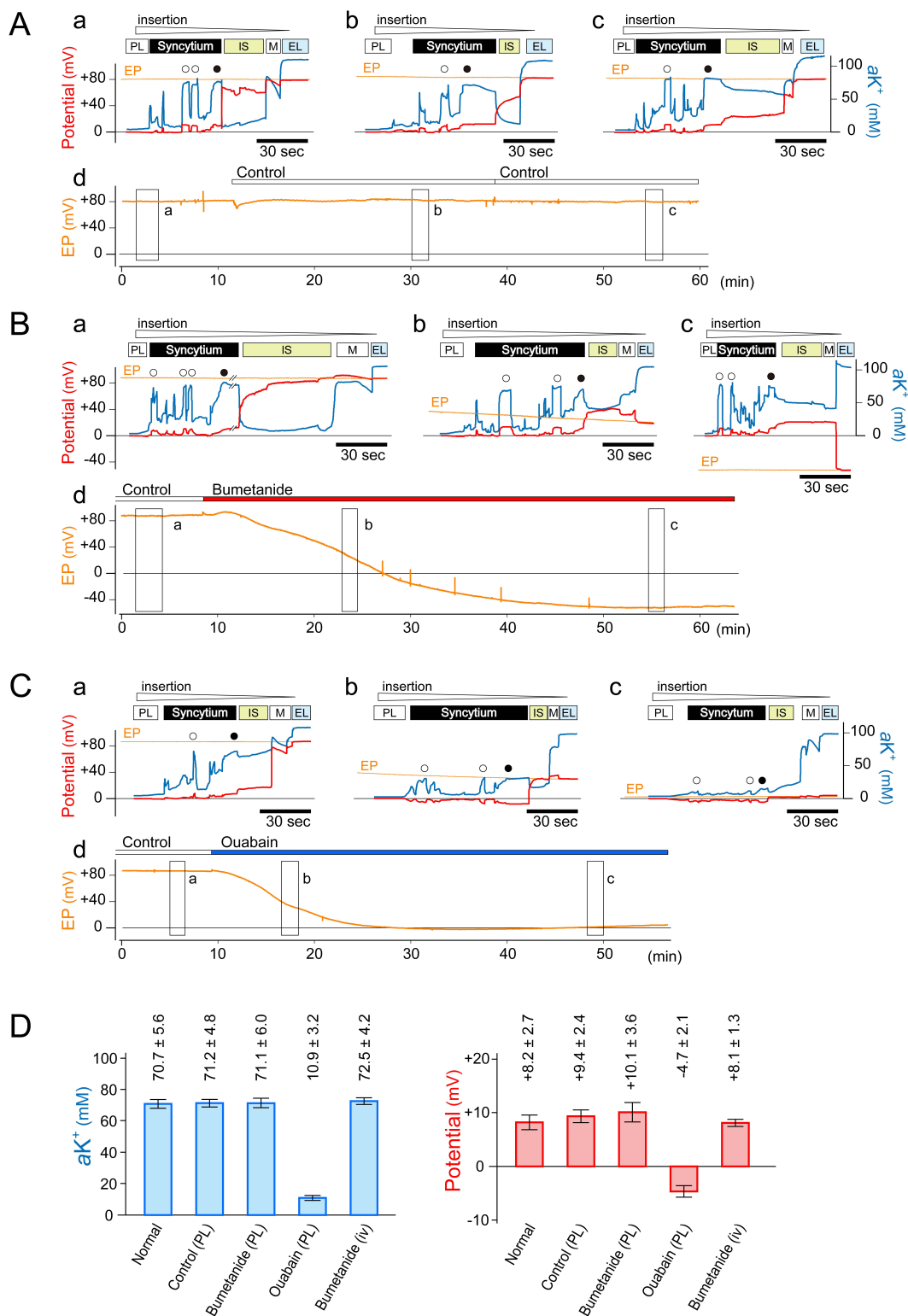vascularis
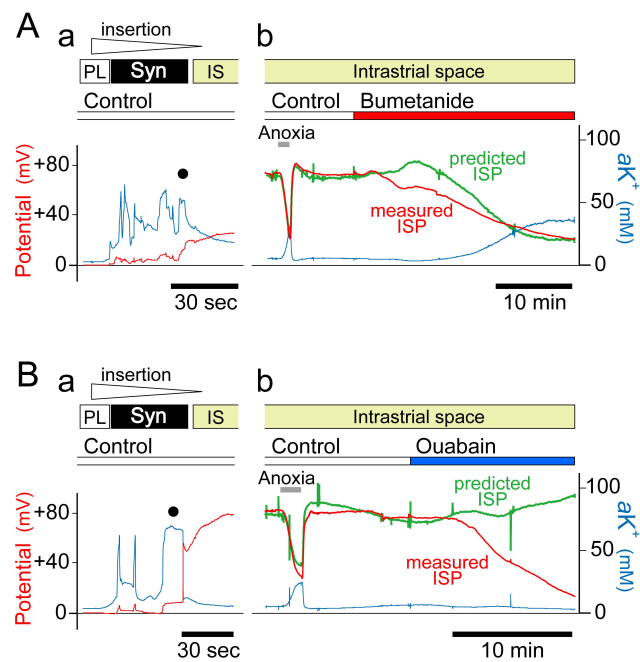
B

Perilymph
(Scala vestibuli)
0 mV, 5 mM [K⁺]

Endolymph
(Scala media)
+80 mV, 150 mM [K⁺]

K⁺

Hair cells

Spiral
ligament

Basilar membrane

Lateral
cochlear
wall

Perilymph (Scala tympani)

B

Spiral
ligament

Stria vascularis

Capillary

Gap
junctions

TJ

Na⁺,K⁺-ATPase

Na⁺,K⁺-ATPase

2 K⁺
3 Na⁺

2 K⁺
3 Na⁺

K⁺

Na⁺

Na⁺
K⁺
2Cl⁻

K⁺

K⁺
2Cl⁻

NKCC

Kir 4.1

I_Ks

NKCC

Cl⁻

ClC

MC

Fibrocytes

TJ
BC

IC

TJ

baso   api

baso   api

Perilymph	Syncytium	Intrastrial space (IS)	Marginal cells	Endolymph

Potential (mV)

0 mV

+7

+90
(ISP)

+80
(EP)

aK⁺ (mM)

Fig. 2

Fig. 3

Fig. 4

Fig. 5